

Cite as: X. Bao, D. W. Eaton, *Science*
10.1126/science.aag2583 (2016).

Fault activation by hydraulic fracturing in western Canada

Xuwei Bao and David W. Eaton*

Department of Geoscience, University of Calgary, Calgary, Alberta T1N 1N4, Canada.

*Corresponding author. E-mail: eatond@ucalgary.ca

Hydraulic fracturing has been inferred to trigger the majority of injection-induced earthquakes in western Canada, in contrast to the midwestern United States where massive saltwater disposal is the dominant triggering mechanism. A template-based earthquake catalog from a seismically active Canadian shale play, combined with comprehensive injection data during a 4-month interval, shows that earthquakes are tightly clustered in space and time near hydraulic fracturing sites. The largest event [moment magnitude (M_w) 3.9] occurred several weeks after injection along a fault that appears to extend from the injection zone into crystalline basement. Patterns of seismicity indicate that stress changes during operations can activate fault slip to an offset distance of >1 km, whereas pressurization by hydraulic fracturing into a fault yields episodic seismicity that can persist for months.

The rate of earthquakes induced by fluid injection from oil and gas operations in parts of North America has surged in recent years (1, 2). In many areas, this increase is primarily associated with high-rate injection of large volumes of saltwater into porous rock formations (3–5). However, the U.S., U.K., and Canada each have well documented earthquakes induced by hydraulic fracturing of low-permeability shale formations, with reported moment magnitudes (M_w) ranging from 2.0 to 4.6 (6–9). Seismicity triggered by hydraulic fracturing appears to be strongly localized. In western Canada, for example, induced seismicity of $M_w \geq 3$ is associated with only ~0.3% of hydraulically fractured wells (2).

While we understand the basic principles of injection-induced seismicity (10, 11), critical details remain incomplete concerning activation of rupture on a fluid-pressurized fault. For massive saltwater injection into a permeable layer, we believe the primary triggering mechanism is an increase in pore pressure within an expanding subsurface volume, which tends to destabilize pre-existing faults by shifting stress conditions into the shear-failure regime (1, 10). The fault-activation process is less clear in the case of hydraulic fracturing, where injection usually occurs within a highly impermeable layer, inhibiting diffusive transport of injected fluids and/or pore pressure (2). Moreover, earthquake nucleation requires unstable slip conditions on a fault, as resistance to sliding must diminish faster than elastic unloading during fault slip. Yet current rate-and-state constitutive laws for rock friction favor aseismic slip in response to increasing pore-fluid pressure (12, 13). Resolving these apparent inconsistencies and developing valid predictive models for earthquakes induced by hydraulic fracturing remain important challenges.

Intermittent sequences of induced earthquakes began in

December 2013 within a region of previous seismic quiescence west of Fox Creek, Alberta (Fig. 1). These earthquake sequences exhibit clear spatial and temporal correlation with hydraulic fracturing of the upper Devonian Duvernay Formation (9), a prolific hydrocarbon source rock that consists of organic-rich mudstone, interfingered with impermeable limestone (14). In response to increased levels of seismicity, real-time seismographic monitoring in this area has been enhanced by the installation of a network of broadband stations (15). In the present study, this network is supplemented by data from 4 broadband seismograph stations installed by an oil and gas operator within the most seismically active part of this region (Fig. 2). The application of algorithms for template-based matched filtering (16) and double-difference relocation (17) has yielded improved magnitude detection threshold and better focal-depth resolution than has heretofore been achieved using regional observations.

In order to undertake a comprehensive comparison between seismicity and injection parameters, we compiled injection data for all wells that were completed in the Duvernay zone from December 2014 to March 2015 (18). At six drilling locations (well pads), hydraulic fracturing was performed in multiple stages within horizontal wellbores. Virtually all of the induced seismicity occurred in spatial clusters concentrated within a lateral distance of ~2 km from hydraulically fractured wells (Fig. 2), with sparse detectable earthquake activity in the intervening areas between clusters. Although no template events were available with which to detect small earthquakes between clusters, even without such template events we can confidently exclude inter-cluster seismicity of magnitude greater than M_w 2.0 based on the detection characteristics of the local array. As argued by previous authors on the basis of temporal and

spatial correlation (2, 9), it is highly unlikely that seismicity in this area has been primarily induced by saltwater injection. For example, to the end of the time interval for this study there was only one saltwater disposal well operating in this area (Fig. 2), injecting into a layer that is higher in the stratigraphic succession (Mississippian Debolt Formation). After three years of operation to the end of March 2015, the cumulative injected volume at the disposal well was only $9.94 \times 10^4 \text{ m}^3$, a small volume compared to other regions where induced seismicity from saltwater disposal has been documented (19).

For the most part, observed induced seismicity exhibits a clear temporal correlation with hydraulic-fracturing activities. As evident from graphs of daily average injection pressure and cumulative injected volume (Fig. 3), most of the induced seismicity occurred during hydraulic-fracturing operations at proximal well pads. Cluster 1 is an exception to this behavior and was seismically active from early January to late March. Persistent but intermittent seismicity within this cluster lacks any clear indication of Omori-type decay in seismicity rate, which is generally characteristic of earthquake aftershock sequences; instead, it is characterized by three distinct post-treatment event sequences (S1-S3), each defined by a pattern of increasing/ decreasing event magnitudes followed by a brief hiatus. The largest induced earthquake (M_w 3.9) took place on 23 January 2015 during sequence S1, two weeks after completion of hydraulic fracturing at pad 1. This event occurred during flowback, a post-injection process during which fracturing fluid is partially recovered in a controlled manner (20). This timing invites speculation that the earthquake was triggered by fluid withdrawal; however, only ~7% of the injected fluids at well 1 flowed back to the wellhead, an unusually low recovery level compared to typical values of ~50% in other parts of western Canada (21). This limited recovery of flowback fluids is indicative of fluid retention within a subsurface region that is in hydrological contact with the primary or secondary network of induced hydraulic fractures (22).

The combined availability of a relatively complete earthquake catalog and comprehensive injection data enable accurate determination of several important parameters. For example, an often-cited relationship postulates that maximum seismic moment for injection-induced earthquakes is limited to the product of the net volume of injected fluid and the effective modulus of rigidity that describes the fault zone (19). This model assumes that the stimulated rockmass is fully saturated, proximal faults are critically stressed, brittle failure occurs within a volume that is weakened by anthropogenic pore pressure increase, and induced earthquakes follow a Gutenberg-Richter magnitude distribution with a b -value near unity. Based on the cumulative injected volume for each well pad, we used this relationship to calculate a time-

dependent upper limit for moment magnitude. The calculated envelope is in general agreement with our observations (Fig. 3). Similarly, the seismogenic index (Σ), defined as $\log_{10} N_{\geq M}(t) - \log_{10} V_I(t) + bM$, provides a measure of site-specific seismotectonic characteristics that expresses the (time independent) potential for induced seismicity per unit injected fluid volume (23). For a given location, calculation of Σ requires observations of the earthquake magnitude-frequency distribution, the b parameter of the Gutenberg-Richter scaling law, and the net injected fluid volume, V_I . The calculated seismogenic index for our study area ranges between -2.7 and -1.5 . These values of Σ exceed values obtained elsewhere for hydraulic fracturing (-9.4 to -4.4), but fall within a previously documented range (23) for geothermal reservoirs (-3.2 to 0.4), suggesting that seismic hazard in the Fox Creek area may be more typical of that for geothermal projects than for other shale plays.

An east-west cross section through cluster 1, where the station geometry is most optimal for determination of precise focal hypocenter locations, reveals two distinct, steeply dipping bands of seismicity extending from the injection zone within the Duvernay Formation into the upper part of crystalline basement (Fig. 4). These bands of seismicity are interpreted as en echelon fault strands within a roughly north-south trending strike-slip fault system, a scenario consistent with nodal planes evident from regional focal mechanisms (Fig. 1). Independent support for the existence of such a fault system is provided by statistical analysis of seismicity patterns (24), coupled with geochemical models for widespread dolomitization of the underlying Swan Hills carbonate platform (25) that invoke basement faults as migration pathways for large volumes of dolomitizing fluids. The bulk of seismicity within the east fault strand is located >1 km from the nearest injection well and, similar to the other 5 clusters, this strand was mainly active during hydraulic-fracturing operations.

In contrast, the more proximal west fault strand was repeatedly activated for several months after completion of the treatment program. The hypocenter distribution suggests that the fault zone intersects the Duvernay Formation between the two injection wells. Hydraulic fracturing was performed in these wells using a so-called zipper frac technique, which involves staggered injection stages between two wells (26). Considering that ~93% of injected hydraulic fracturing fluids at well pad 1 were not recovered during flowback, it is likely that sustained pressurization of the fault zone occurred. Induced seismicity sequences appear to have occurred in a retrograde fashion, with the hypocenter of the largest event (sequence S1) located at the deepest level within the upper part of Precambrian crystalline basement, followed by migration of subsequent sequences (S2 and S3) to shallower levels, closer to the injection zone.

A recent analytical study that considered poroelastic coupling of stress and pore pressure in a homogeneous medium shows that, at large distances from a fluid injection site, stresses ultimately dominate over pore-pressure increase (27). Similarly, a numerical analysis, also based on poroelasticity theory, suggests that a 2013–2014 episode of seismicity induced by hydraulic fracturing in the Fox Creek area is best explained by the elastic response of the solid matrix, rather than fluid diffusion (28). In our study, the east and west strands of cluster 1 appear to delineate faults with similar orientations but contrasting activation signatures. As shown in fig. S10 of the supplementary materials, when the elastic response of the surrounding medium to hydraulic fracturing at well pad 1 is considered, seismicity within the east strand largely falls within a positive Coulomb stress-change regime (up to ~ 0.1 MPa), consistent with previous findings (28). On the other hand, hypocenters for the west strand fall largely within a regime wherein elastic stresses induced by hydraulic fracturing are predicted to inhibit fault slip, implying that a different triggering mechanism is required.

According to a model for nucleation and arrest of dynamic rupture on a pressured fault (29), the existence of a permeable and aeri ally extensive fault that is imperfectly aligned with the optimal orientation within the regional stress field enables pressurization to occur over a large fault patch prior to nucleation of rupture. As shown in fig. S11 of the supplementary materials, post-injection activation of the M_w 3.9 earthquake is consistent with pore-pressure diffusion along the west fault strand. Taken together, our observations suggest that: (i) a \sim two-week delay in occurrence of the largest event after completion of hydraulic fracturing corresponds with relatively aseismic pressure diffusion on the west fault strand; (ii) earthquake nucleation occurred within the uppermost crystalline basement and was triggered by an estimated pore-pressure change of ~ 0.12 MPa; (iii) the slip regime within the weakened, fluid-pressurized fault segment above the initial rupture during sequence S1 was subject to re-nucleation during sequences S2 and S3, months after elastic stresses from the hydraulic fracturing operations had subsided based on lack of seismicity within the east fault strand.

The occurrence of the M_w 3.9 earthquake on 23 January 2015 prompted, shortly thereafter, the introduction of new regulations applicable to this region that include a “traffic light protocol” that mandates immediate shutdown in hydraulic fracturing operations following an earthquake of M_L (local magnitude) 4.0 or greater within 5 km of an affected well (30). Similar magnitude-based traffic-light protocols have been established in other jurisdictions (31). As seen in many studies of injection-induced seismicity from massive saltwater disposal, in this study a reactivated fault zone is

imaged by well-located hypocenters. Our results indicate that fault activation during and after hydraulic fracturing can be triggered by different mechanisms, including stress changes due to the elastic response of the rockmass to hydraulic fracturing or pore-pressure changes due to fluid diffusion along a permeable fault zone. While stress-related triggering appears to diminish shortly after operations, a fluid-pressurized fault may be susceptible to persistent seismicity for a period of at least several months. This suggests that increased sensitivity of a fluid-pressurized fault should be considered in ongoing development of mitigation strategies for seismicity induced by hydraulic fracturing.

References and Notes

1. W. L. Ellsworth, Injection-induced earthquakes. *Science* **341**, 1225942 (2013). [doi:10.1126/science.1225942](https://doi.org/10.1126/science.1225942) [Medline](#)
2. G. M. Atkinson, D. W. Eaton, H. Ghofrani, D. Walker, B. Cheadle, R. Schultz, R. Shcherbakov, K. Tiampo, J. Gu, R. M. Harrington, Y. Liu, M. van der Baan, H. Kao, Hydraulic fracturing and induced seismicity in the Western Canada Sedimentary Basin. *Seismol. Res. Lett.* **87**, 631–647 (2016). [doi:10.1785/0220150263](https://doi.org/10.1785/0220150263)
3. C. Frohlich, Two-year survey comparing earthquake activity and injection-well locations in the Barnett Shale, Texas. *Proc. Natl. Acad. Sci. U.S.A.* **109**, 13934–13938 (2012). [doi:10.1073/pnas.1207728109](https://doi.org/10.1073/pnas.1207728109) [Medline](#)
4. K. M. Keranen, M. Weingarten, G. A. Abers, B. A. Bekins, S. Ge, Sharp increase in central Oklahoma seismicity since 2008 induced by massive wastewater injection. *Science* **345**, 448–451 (2014). [doi:10.1126/science.1255802](https://doi.org/10.1126/science.1255802) [Medline](#)
5. M. Weingarten, S. Ge, J. W. Godt, B. A. Bekins, J. L. Rubinstein, High-rate injection is associated with the increase in U.S. mid-continent seismicity. *Science* **348**, 1336–1340 (2015). [doi:10.1126/science.aab1345](https://doi.org/10.1126/science.aab1345) [Medline](#)
6. A. Holland, Earthquakes triggered by hydraulic fracturing in south-central Oklahoma. *Bull. Seismol. Soc. Am.* **103**, 1784–1792 (2013). [doi:10.1785/0120120109](https://doi.org/10.1785/0120120109)
7. H. Clarke, L. Eisner, P. Styles, P. Turner, Felt seismicity associated with shale gas hydraulic fracturing: The first documented example in Europe. *Geophys. Res. Lett.* **41**, 8308–8314 (2014). [doi:10.1002/2014GL062047](https://doi.org/10.1002/2014GL062047)
8. R. Skoumal, M. Brudzinski, B. Currie, Earthquakes induced by hydraulic fracturing in Poland Township, Ohio. *Bull. Seismol. Soc. Am.* **105**, 189–197 (2015). [doi:10.1785/0120140168](https://doi.org/10.1785/0120140168)
9. R. Schultz, V. Stern, M. Novakovic, G. Atkinson, Y. Gu, Hydraulic fracturing and the Crooked Lake Sequences: Insights gleaned from regional seismic networks. *Geophys. Res. Lett.* **42**, 2750–2758 (2015). [doi:10.1002/2015GL063455](https://doi.org/10.1002/2015GL063455)
10. M. K. Hubbert, W. W. Rubey, Role of fluid pressure in mechanics of overthrust faulting I. Mechanics of fluid-filled porous solids and its application to overthrust faulting. *Geol. Soc. Am. Bull.* **70**, 115–166 (1959).
11. C. B. Raleigh, J. H. Healy, J. D. Bredehoeft, An experiment in earthquake control at Rangely, Colorado. *Science* **191**, 1230–1237 (1976). [doi:10.1126/science.191.4233.1230](https://doi.org/10.1126/science.191.4233.1230) [Medline](#)
12. Y. Guglielmi, F. Cappa, J. P. Avouac, P. Henry, D. Elsworth, Seismicity triggered by fluid injection-induced aseismic slip. *Science* **348**, 1224–1226 (2015). [doi:10.1126/science.aab0476](https://doi.org/10.1126/science.aab0476) [Medline](#)
13. M. M. Scuderi, C. Collettini, The role of fluid pressure in induced vs. triggered seismicity: Insights from rock deformation experiments on carbonates. *Sci. Rep.* **6**, 24852 (2016). [doi:10.1038/srep24852](https://doi.org/10.1038/srep24852) [Medline](#)
14. S. Creaney, J. Allan, K. S. Kole, M. G. Fowler, P. W. Brooks, K. G. Osadetz, R. W. Macqueen, L. R. Snowdon, C. L. Riediger, Petroleum generation and migration in the western Canada sedimentary basin. in *Geological Atlas of the Western Canada Sedimentary Basin*, G.D. Mossop and I. Shetsen (comp.) (Canadian Society of Petroleum Geologists and Alberta Research Council, 1994).
15. R. Schultz, V. Stern, Y. J. Gu, D. Eaton, Detection threshold and location resolution of the Alberta Geological Survey earthquake catalogue. *Seismol. Res. Lett.* **86** (2A), 385–397 (2015). [doi:10.1785/0220140203](https://doi.org/10.1785/0220140203)
16. E. Caffagni, D. W. Eaton, J. P. Jones, M. van der Baan, Detection and analysis of microseismic events using a Matched Filtering Algorithm (MFA). *Geophys. J. Int.*

- ggw168 (2016). doi:10.1093/gji/ggw168
17. F. Waldhauser, W. Ellsworth, A double-difference earthquake location algorithm: Method and application to the northern Hayward Fault, California. *Bull. Seismol. Soc. Am.* **90**, 1353–1368 (2000). doi:10.1785/0120000006
 18. Materials and methods are available as supplementary materials on Science Online.
 19. A. McGarr, Maximum magnitude earthquakes induced by fluid injection. *J. Geophys. Res.* **119**, 1008–1019 (2014). doi:10.1002/2013JB010597
 20. K. B. Gregory, R. D. Vidic, D. A. Dzombak, Water management challenges associated with the production of shale gas by hydraulic fracturing. *Elements* **7**, 181–186 (2011). doi:10.2113/gselements.7.3.181
 21. BC Oil and Gas Commission, "Investigation of observed seismicity in the Montney Trend." (BC Oil and Gas Commission, Fort St John, British Columbia, 2014).
 22. M. M. Sharma, R. Manchanda, The role of induced un-propped (IU) fractures in unconventional oil and gas wells. in *SPE Annual Technical Conference and Exhibition*, 28–30 September 2014, Houston, TX (SPE-174946-MS, Society of Petroleum Engineers, Richardson, TX, 2015).
 23. C. Dinske, S. A. Shapiro, Seismotectonic state of reservoirs inferred from magnitude distributions of fluid-induced seismicity. *J. Seismol.* **17**, 13–25 (2013). doi:10.1007/s10950-012-9292-9
 24. R. Schultz, H. Corlett, K. Haug, K. Kocon, K. MacCormack, V. Stern, T. Shipman, Linking fossil reefs with earthquakes: Geologic insight to where induced seismicity occurs in Alberta. *Geophys. Res. Lett.* **43**, 2534–2542 (2016). doi:10.1002/2015GL067514
 25. D. Green, E. Mountjoy, Fault and conduit controlled burial dolomitization of the Devonian west-central Alberta Deep Basin. *Bull. Can. Pet. Geol.* **53** (2), 101–129 (2005). doi:10.2113/53.2.101
 26. M. Rafiee, M. Y. Soliman, E. Pirayesh, Hydraulic fracturing design and optimization: a modification to zipper frac. In *SPE Annual Technical Conference and Exhibition*, 8–10 October, San Antonio, TX (SPE-159786-MS, Society of Petroleum Engineers, Richardson, TX, 2012)
 27. P. Segall, S. Lu, Injection-induced seismicity: Poroelastic and earthquake nucleation effects. *J. Geophys. Res. Solid Earth* **120**, 5082–5103 (2015). doi:10.1002/2015JB012060
 28. K. Deng, Y. Liu, R. M. Harrington, Poroelastic stress triggering of the December 2013 Crooked Lake, Alberta, induced seismicity sequence. *Geophys. Res. Lett.* **43**, 8482–8491 (2016). doi:10.1002/2016GL070421
 29. D. I. Garagash, L. N. Germanovich, Nucleation and arrest of dynamic slip on a pressurized fault. *J. Geophys. Res.* **117** (B10), B10310 (2012). doi:10.1029/2012JB009209
 30. Alberta Energy Regulator, Subsurface order no. 2, 19 February 2015.
 31. R. J. Walters, M. D. Zoback, J. W. Baker, G. C. Beroza, Characterizing and responding to seismic risk associated with earthquakes potentially triggered by fluid disposal and hydraulic fracturing. *Seismol. Res. Lett.* **86**, 1110–1118 (2015). doi:10.1785/0220150048
 32. H. Zhang, D. W. Eaton, G. Li, Y. Liu, R. M. Harrington, Discriminating induced seismicity from natural earthquakes using moment tensors and source spectra. *J. Geophys. Res. Solid Earth* **121**, 972–993 (2016). doi:10.1002/2015JB012603
 33. R. Wang, Y. J. Gu, R. Schultz, A. Kim, G. M. Atkinson, Source analysis of a potential hydraulic-fracturing-induced earthquake near Fox Creek, Alberta. *Geophys. Res. Lett.* **43**, 564–573 (2016). doi:10.1002/2015GL066917
 34. Trans Alta catalog of Nanometrics, Ltd.
 35. D. R. Shelly, G. C. Beroza, S. Ide, Non-volcanic tremor and low-frequency earthquake swarms. *Nature* **446**, 305–307 (2007). doi:10.1038/nature05666 [Medline](#)
 36. G. Laske, G. Masters, Z. Ma, M. Pasyanos, Update on CRUST1.0—A 1-degree global model of Earth's crust. *Geophys. Res. Abstracts* **15**, abstr. EGU2013-2658 (2013).
 37. J. Schweitzer, HYPOSAT – An Enhanced Routine to Locate Seismic Events. *Pure Appl. Geophys.* **158**, 277–289 (2001). doi:10.1007/PL00001160
 38. Z. H. El-Isa, D. W. Eaton, Spatiotemporal variations in the *b*-value of earthquake magnitude–frequency distributions: Classification and causes. *Tectonophysics* **615–616**, 1–11 (2014). doi:10.1016/j.tecto.2013.12.001
 39. O. Heidbach, M. Tingay, A. Barth, J. Reinecker, D. Kurfeß, B. Müller, Global crustal stress pattern based on the World Stress Map database release 2008. *Tectonophysics* **482**, 3–15 (2010). doi:10.1016/j.tecto.2009.07.023
 40. C. P. King, R. S. Stein, J. Lin, Static stress changes and the triggering of earthquakes. *Bull. Seismol. Soc. Am.* **84**, 935–953 (1994).
 41. R. S. Stein, The role of stress transfer in earthquake occurrence. *Nature* **402**, 605–609 (1999). doi:10.1038/45144
 42. N. Boroumand, D. W. Eaton, Energy-based hydraulic fracture numerical simulation: Parameter selection and model validation using microseismicity. *Geophysics* **80**, W33–W44 (2015). doi:10.1190/geo2014-00911
 43. Y. Okada, Internal deformation due to shear and tensile faults in a half-space. *Bull. Seismol. Soc. Am.* **82**, 1018–1040 (1992).
 44. Canadian Discovery, The Duvernay Project: Gas Liquids and Geomechanics (2015).
 45. N. J. van der Elst, H. M. Savage, K. M. Keranen, G. A. Abers, Enhanced remote earthquake triggering at fluid-injection sites in the midwestern United States. *Science* **341**, 164–167 (2013). doi:10.1126/science.1238948 [Medline](#)
 46. B. Wang, R. M. Harrington, Y. Liu, H. Yu, A. Carey, N. J. van der Elst, Isolated cases of remote dynamic triggering in Canada detected using cataloged earthquakes combined with a matched-filter approach. *Geophys. Res. Lett.* **42**, 5187–5196 (2015). doi:10.1002/2015GL064377
 47. K. Aki, Maximum likelihood estimate of *b* in the formula $\log N = a - bM$ and its confidence limits. *Bull. Earthquake Res. Inst.* **43**, 237–239 (1965).

Acknowledgments

Funding for this study was provided by the Natural Sciences and Engineering Research Council of Canada (grant IRCSA 485691), Chevron Canada Resources, Ltd. and the University of Calgary. Telemetered data from the Regional Alberta Observatory for Earthquake Studies Network (RAVEN) operated by the Alberta Geological Survey were used in this study. Facilities of IRIS Data Services were used to access waveforms from the RAVEN network. Seismographic data from four additional broadband stations, as well as flowback data for well pad 1, were provided by Repsol Canada. These four stations were installed and operated by Nanometrics, Ltd. Injection pressures and volumes were accessed under license from the Well Completions and Frac Database, owned and licensed by Canadian Discovery Ltd. The injection data can also be accessed online through the Alberta Energy Regulator at <http://aer.ca/>, using the well ID numbers listed in the supplementary material. Generic Mapping Tools (GMT) was used to prepare several figures. Calculated earthquake magnitudes, hypocenter locations and injection data are provided as supplementary material. X.B. and D.W.E. both warrant that they have no conflict of interest in this work.

Supplementary Materials

www.sciencemag.org/cgi/content/full/science.aag2583/DC1
 Materials and Methods
 Figures S1 to S11
 Tables S1 to S7
 References (35–47)

31 May 2016; resubmitted 20 June 2016

Accepted 21 October 2016

Published online 17 November 2016

10.1126/science.aag2583

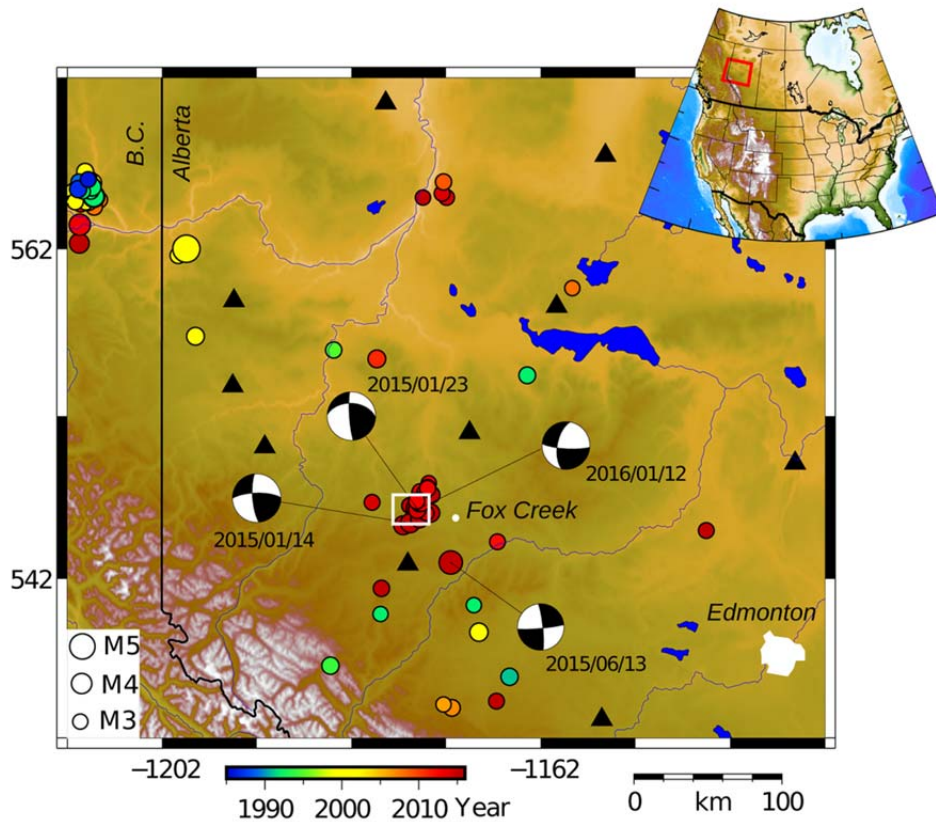


Fig. 1. Seismicity of northwestern Alberta, Canada for the period 1985–2016. Symbol size indicates magnitude and color denotes date of occurrence. Seismicity west of Fox Creek commenced in December 2013, and correlates in space and time with local hydraulic-fracturing operations (9). Focal mechanisms of the largest earthquakes, from (32–34), are labeled by year/month/date of occurrence. White rectangle outlines the area in Fig. 2.

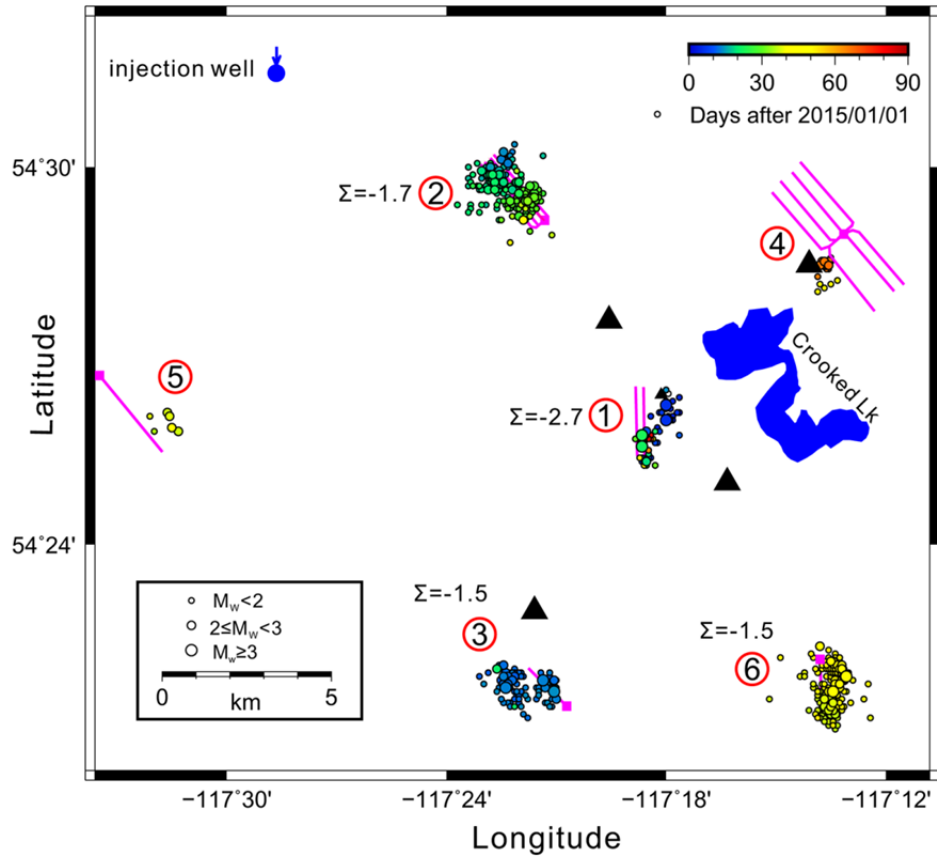


Fig. 2. Details of seismicity induced by hydraulic fracturing at 6 well pads from December 2014 to March 2015. Black triangles show local broadband seismograph stations; small black triangle shows a station that was deployed for a short time after the M_w 3.9 event. Event symbols are colored by date of occurrence and are scaled based on magnitude. Well pads are numbered sequentially by initiation of hydraulic-fracturing operations.

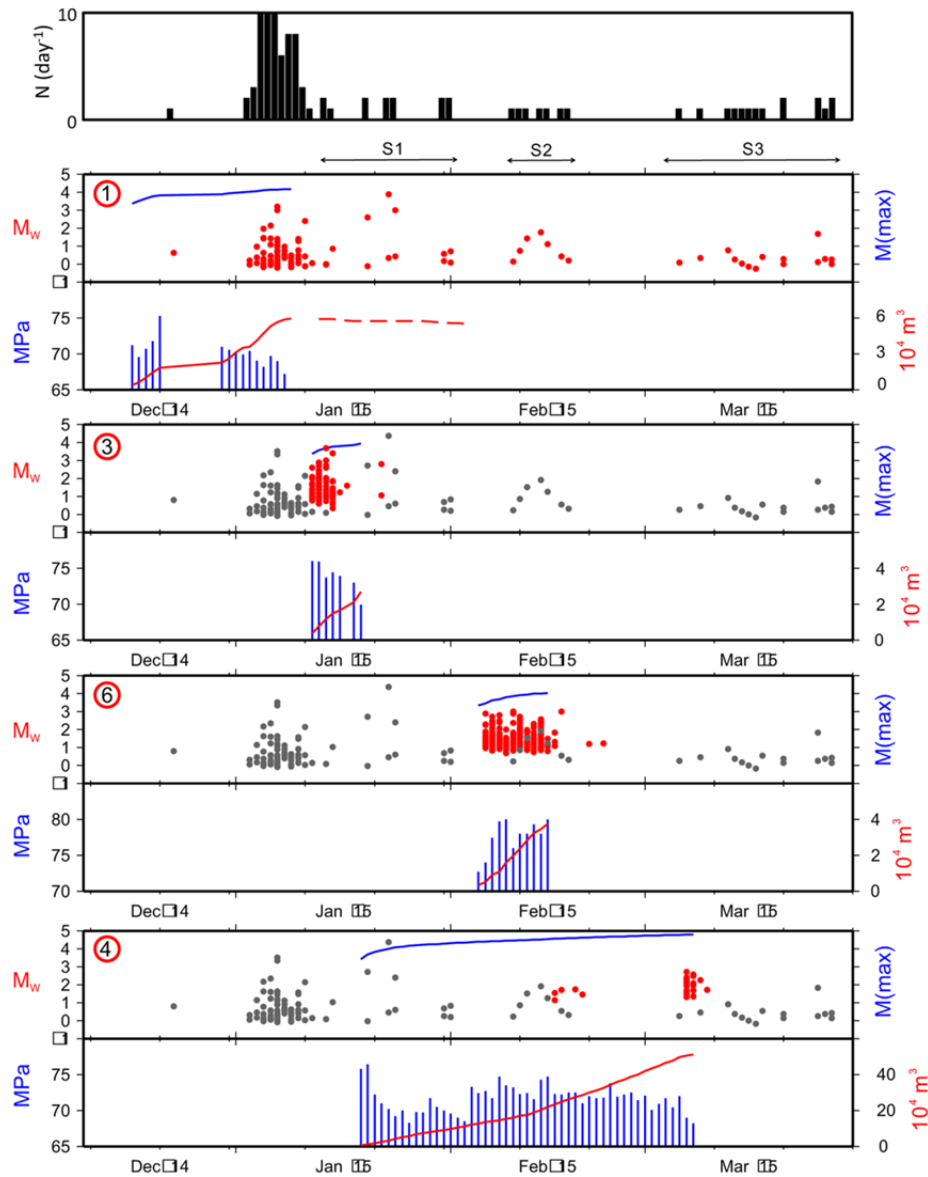


Fig. 3. Comparison of seismicity and injection schedules for selected clusters. For each cluster (numbered as in Fig. 2), the upper panel shows seismicity (red dots) and calculated maximum magnitude (blue curve) (19), while the lower panel shows average daily treatment pressure (blue bars) and cumulative injected volume (red curve). Cluster 1 seismicity is repeated as gray dots in other graphs, for timing comparison. Black bar graph at top shows number of events per day for cluster 1, which lacks a typical Omori decay. At well 1, flowback (dashed curve) indicates recovery of only 7% of injected fluid. S1–S3 indicates time windows for interpreted sequences. A complete set of graphs for all clusters is shown in supplementary materials (fig. S9).

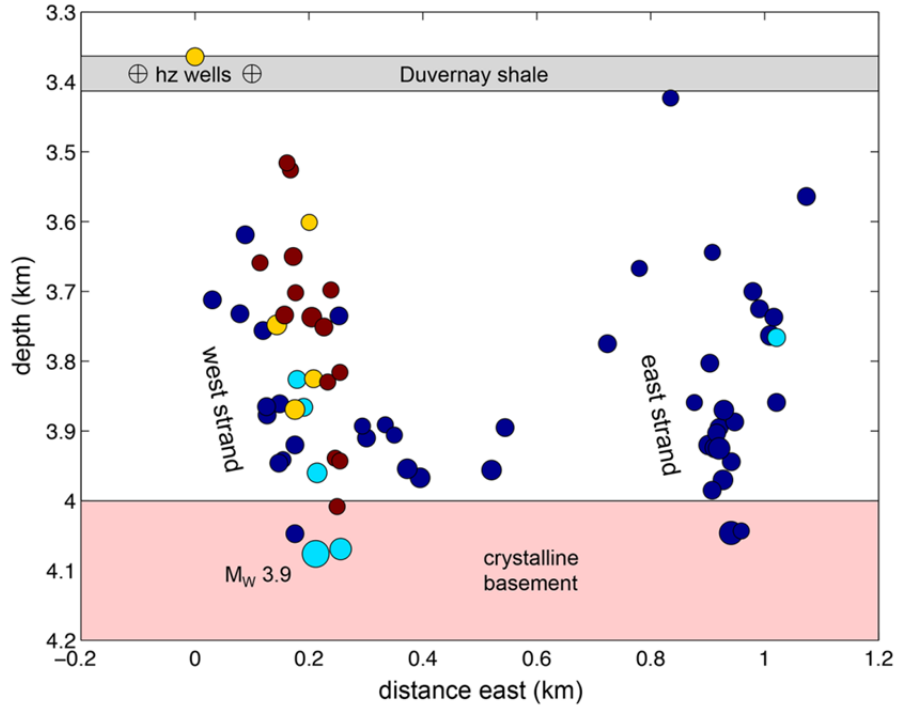


Fig. 4. Cross section through cluster 1, showing east and west fault strands inferred from double-difference event locations. Dark blue symbols show events that occurred during hydraulic fracturing in two horizontal (hz) wells. Light blue, yellow and red symbols show subsequent events during sequences S1, S2 and S3, respectively.

EXTENDED PDF FORMAT
SPONSORED BY



Fault activation by hydraulic fracturing in western Canada
Xuewei Bao and David W. Eaton (November 17, 2016)
published online November 17, 2016

Editor's Summary

This copy is for your personal, non-commercial use only.

- Article Tools** Visit the online version of this article to access the personalization and article tools:
<http://science.sciencemag.org/content/early/2016/11/16/science.aag2583>
- Permissions** Obtain information about reproducing this article:
<http://www.sciencemag.org/about/permissions.dtl>

Science (print ISSN 0036-8075; online ISSN 1095-9203) is published weekly, except the last week in December, by the American Association for the Advancement of Science, 1200 New York Avenue NW, Washington, DC 20005. Copyright 2016 by the American Association for the Advancement of Science; all rights reserved. The title *Science* is a registered trademark of AAAS.